11th U.S. National Combustion Meeting
Organized by the Western States Section of the Combustion Institute
March 24–27, 2019
Pasadena, California

Direct numerical simulation of an auto-ignitive turbulent flame in a stratified dimethyl-ether (DME)/air mixture

Swapnil Desai[1,*], *Ramanan Sankaran*[2], *and Hong G. Im*[3]

[1]*Bredesen Center for Interdisciplinary Research and Graduate Education, University of Tennessee, Knoxville, TN 37996-3394, USA*
[2]*Oak Ridge National Laboratory, Oak Ridge, TN 37831-6008, USA*
[3]*Clean Combustion Research Center, King Abdullah University of Science and Technology, Thuwal 23955-6900, Saudi Arabia*
[*]*Corresponding author:* swapnildesai1989@gmail.com

Abstract: Direct numerical simulations (DNS) of a turbulent premixed flame in an auto-ignitive dimethyl-ether (DME)/air mixture exhibiting two-staged ignition were conducted at elevated pressure and temperature using a statistically stationary planar configuration. Three sets of conditions with an identical turbulence intensity, but different stratification/turbulence length scales and correlations between temperature (T) and equivalence ratio (ϕ) fields were simulated to study the dynamics of turbulent premixed flame propagation at auto-ignitive conditions. The influence of different stratification length scales and T-ϕ correlations on turbulent flame speed was examined by comparing the flame statistics obtained from 2D simulations against laminar 1D solution. A global analysis of the front propagation speed was carried out for determining the effect of turbulent wrinkling and the role of upstream auto-ignition on the overall burning rate.
Keywords: Flame dynamics, Two-stage ignition, Turbulent flame speed, Thermal and composition stratification

1. Introduction

Turbulent premixed flames play a major role in modern combustion devices such as internal combustion engines and gas turbine combustors. Since these devices operate at elevated pressures and temperatures, they often encompass mixed modes of combustion, in which flames and auto-ignition processes are simultaneously contributing to combustion and heat release ([1, 2] and references therein). The presence of such dual combustion modes poses engineering challenges in precise control of combustion phasing. To improve upon this control issue, some degree of stratification is deliberately introduced to avoid extremely rapid pressure rise and heat release rates. Exhaust gas re-circulation and multiple fuel injection are some of the techniques that are employed to introduce charge stratification in the combustion chamber. Moreover, some thermal stratification always exists in the combustion chamber due to wall heat loss. Depending on the fuel injection timing, exhaust gas re-circulation and the amount of wall heat loss, different correlations may occur between temperature (T) and equivalence ratio (ϕ) prior to major heat release event. Essentially, it is plausible to think of two limiting scenarios: 1) early start of injection may result in largely uncorrelated T and ϕ fields mostly due to turbulence mixing and wall heat loss; and 2) late start of

fuel injection may result in negatively correlated T and ϕ fields mostly due to evaporative cooling. Insufficient mixing between hot residual gas which contain oxygen and the fresh charge can also result in a negatively correlated T and ϕ fields. Due to the presence of turbulence, large scale stratification of charge leads to small scale inhomogeneities in both temperature and fuel mass fraction. Additionally, these devices utilize large hydrocarbon fuels such as gasoline, diesel and jet fuels which have a strong low temperature chemistry (LTC) behavior. As such, not only the turbulence chemistry but also the fuel chemistry and molecular transport are expected to play an important role in affecting turbulent combustion. The mode as well as speed of a reaction front under such conditions still remains unclear.

There has been a number of studies of turbulent premixed flames in which the role of turbulent intensity on flame burning velocities and flame structures has been the major focus [3–7]. The effects of pressure [8], Lewis number [9], preferential diffusion [10], turbulent flame geometry [11], equivalence ratio [12] and unburnt temperature [13, 14] on turbulent flame propagation have also been examined. All these studies employed a turbulent flame regime diagram called the Borghi diagram to provide insightful information for different flame regimes [15]. This diagram defines the boundaries between wrinkled, corrugated, thin reaction zone and distributed reaction zone flames based on the ratio of turbulence scales to characteristic flame scales. However, these turbulent flame studies as well as the Borghi diagram have been based on the assumption of a chemically frozen flow ahead of the flame. These studies also neglected the effect of low temperature chemistry for transportation fuels at elevated temperatures and pressures [16–18]. Recently, the effect of LTC on turbulent flame speed was investigated experimentally [19, 20]. At a constant turbulence intensity, a significant increase in turbulent flame speed was observed as the mixture underwent first stage ignition. This increase was attributed to an increase in the laminar flame speed and a decrease in fuel Lewis number. Four different turbulent combustion regimes were observed based on the competition of the ignition, flow and flame time scales. These experimental investigations provided initial evidences of non-unique turbulent flame regimes and turbulent flame speeds of fuels which exhibit LTC. Subsequently, direct numerical simulations of cool flames and hot flames propagating in a mixture that has undergone first stage ignition have been recently carried out by Savard et al. [21]. The increase in turbulent flame speed was again attributed to the increase in laminar flame speed, as opposed to turbulence-LTC interaction. With reference to cool flames, it was found that their reaction zone structure approaches that of the reference laminar flame and their normalized turbulent flame speed was found to be comparable to that of hot flames. While this study provided significant insights into the role of low temperature chemistry in turbulent flame propagation, the effects of thermal or composition stratification were not considered. Moreover, under the chosen conditions, there was a large separation between first stage and second stage ignition delay times such that cool flames and hot flames were isolated from one another. As such, a coupled low temperature and high temperature double-flame which has been shown to exist under engine relevant conditions [17, 22, 23] was not considered.

Based on the above discussion, the goal of the present study is: 1) To explain the influence of different stratification length scales and T-ϕ correlations on the dynamics of a 2-staged turbulent premixed DME/air flame at auto-ignitive conditions under an identical turbulent intensity by performing 2-D DNS, 2) To obtain statistical measures of the influence of turbulence and upstream auto-ignition on the global burning velocity of the flame by determining the individual contributions of flame wrinkling (A') and the enhancement of burning rate per unit surface area (I_0) to the overall burning rate. We relate the turbulent burning velocity to a one-dimensional propagation

speed through I_0 and A'. Although turbulence is inherently three-dimensional, the present 2D study is a first step in understanding the effects of inhomogeneties in both temperature and equivalence ratio on turbulent flame propagation at conditions which are representative of real engines.

2. Problem configuration

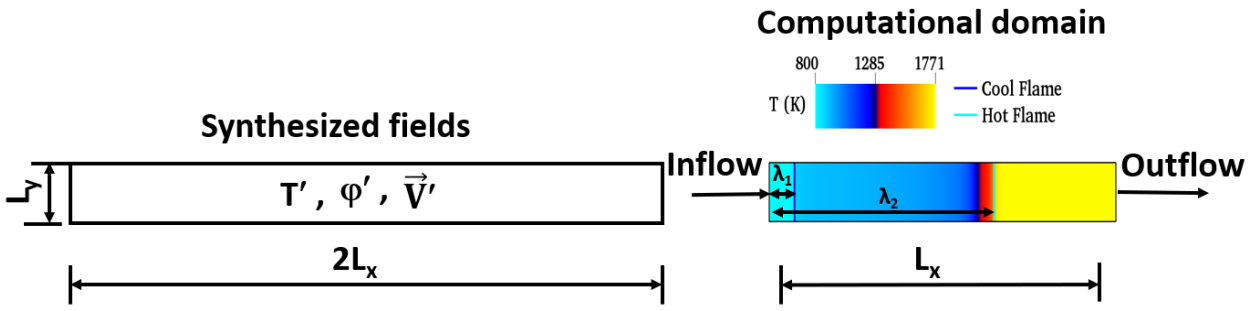

Fig. 1: Schematic diagram of the flow configuration

Fig. 1 presents a schematic diagram of the turbulent flame configuration. A 2D statistically-planar, freely propagating flame with an unburnt mixture temperature of 800 K, ϕ=0.4 and an elevated pressure of 20 atm. was chosen to isolate the effects of turbulence and stratification on the flame from mean flow shear and curvature effects. The simulation was initialized using a laminar solution obtained from Cantera [24] with a fixed inflow velocity of 2 m/s. Periodic boundary condition in the y-direction and non-reflecting inflow and outflow [25] in the x-direction were used. Under the chosen unburnt mixture conditions, a stable freely propagating double-flame could not be obtained as the flame characteristic time was within an order of magnitude from the first-stage ignition delay time. Under such conditions, the laminar flame solution has been found to be strongly dependent on the simulation domain length [18, 26]. As such, at low inflow velocities, a stable flame can only be attached to the inlet. Such a flame cannot be used to initialize turbulent flames while maintaining a sufficient distance from the inlet. Hence, an ignition front propagating at 2 m/s was used. This made it possible to maintain the reaction front at a sufficient distance from the inlet and avoid interference of the boundary conditions. Externally synthesized turbulent flow, composition and temperature fields were then injected at the inlet in addition to the mean inflow velocity, temperature and composition. The initial turbulent flow field was synthesized by using an isotropic kinetic energy spectrum function by Passot-Pouquet [27]. The most energetic turbulence length scale, l_e was varied from 480 μm to 960 μm. In real engines, the turbulence time scale, τ_t is comparable to $\tau_{ignition}$ [28]. Therefore, based on the two homogeneous ignition delay times under the chosen conditions, τ_1 (= 0.48 ms) and τ_2 (= 3.06 ms), velocity fluctuation RMS, u' of 0.4 was selected to match τ_t with $\tau_{ignition}$. Composition and temperature fields were also synthesized from the same energy spectrum as turbulence but with different random seeds. The various physical and numerical parameters used in the present study are listed in Table 1. The location of stabilization of the cool and the hot ignition front from the inlet is denoted by λ_1 (= 0.87 mm) and λ_2 (= 7.43 mm) as shown in Fig. 1. A uniform grid spacing (Δ) of 7.5 μm was sufficient to fully resolve both chemistry (atleast 12 grid points across the thinnest radical reaction rate layer) and turbulence (atleast 12 grid points per Kolomogorov length scale). In all cases, the characteristic length scale

of temperature fluctuations, l_T and the characteristic length scale of composition fluctuations, l_{DME} were selected identical to the most energetic turbulence length scale, l_e so as to have most effective turbulent mixing of the mixture [29]. The case labels suffixed with N had a negatively correlated T-ϕ distribution whereas those suffixed with R had an uncorrelated T-ϕ distribution. The number in the case labels denotes the length scale in μm. The values of temperature fluctuations RMS, T$'$ and the composition fluctuation RMS, ϕ' were chosen such that the range of spatial temperature and composition distribution closely matched the observations of Wang and Rutland [30].

Case	480N	480R	720N	720R	960N	960R
Domain size (L_x, mm x L_y, mm)	11.52 x 1.44		12.96 x 2.16		12.96 x 2.88	
Mesh size (N_x x N_y)	1536 x 192		1728 x 288		1728 x 384	
S_L (m/s)	0.32					
Kolmogorov length scale, l_k (μm) [a]	95		105		112	
Turbulence intensity (u'/S_L)	1.25					
$l_e = l_T = l_{DME}$ (μm)	480		720		960	
Temperature fluctuation RMS, T$'$ (K)	15					
Composition fluctuation RMS, ϕ'	0.1					
Turbulence time scale, τ_t (ms)	1.2		1.8		2.4	
$U_{in} = S_T$ (m/s)	2					

Table 1: Simulation parameters

[a] Kolmogorov length scale, l_k is estimated as $(\nu^3/\varepsilon)^{1/4}$ where $\nu = 4.1 \times 10^{-5}$ m^2/s, is the kinematic viscosity at the inflow conditions and ε is the turbulence energy dissipation rate

3. Numerical method

The simulations were performed using the DNS code KARFS [31], which solves the fully compressible Navier-Stokes, species and energy equations. It uses a fourth-order Runge-Kutta method for time integration, an eighth-order explicit spatial difference scheme for evaluating the diffusive fluxes and a seventh-order mapped WENO [32] scheme for evaluating the convective fluxes. Based on the mean inlet velocity, the flow through time, τ_U, varied from 5.76 ms to 6.48 ms in the respective cases. In each case, the solution was advanced at a constant 10 ns time-step for two flow through times. The first flow through time was neglected from analysis to remove any effects due to initial transients. Data from equally spaced time instants from the remainder of the simulation was used to obtain the statistical results. Averaging was performed in time and the y-direction.

4. Results and Discussion

4.1 1D analysis

To identify a reference laminar flame speed, the method proposed in [26] was followed. A series of steady state flame solutions were evaluated in Cantera [24] by varying the flame position, λ_2 (based on the location of maximum heat release rate), for which the correct inflow velocity, U_{in} was determined as an eigenvalue. Fig. 2 presents λ_1 and λ_2 as a function of U_{in}. The derivative $d\lambda_2/dU_{in}$ vs. U_{in} is also shown. A distinguishable peak in $d\lambda_2/dU_{in}$ can be seen at the inflow velocity of

0.32 m/s. Based on the argument provided in [26], this value corresponds to the reference laminar flame speed, S_L. Based on this value of S_L, the non-dimensional turbulence intensity (u'/S_L) is 1.25. As discussed earlier, the steady propagation speed is highly sensitive to λ_2 under the chosen conditions. Hence, for the unsteady cases, two additional auto-ignitive speeds, $S_{1D,cool}$ and $S_{1D,hot}$ were evaluated based on the time-averaged values of λ_1 and λ_2 as per the above procedure. These were later used to determine the individual contributions from increase in length (A') and from the increase in burning rate per unit length of the flame (I_0) to the overall burning rate of the cool as well as the hot reaction front as per the model suggested by Bray [33], Candel and Poinsot [34]: $S_T/S_{1D} = I_0 \cdot A'$.

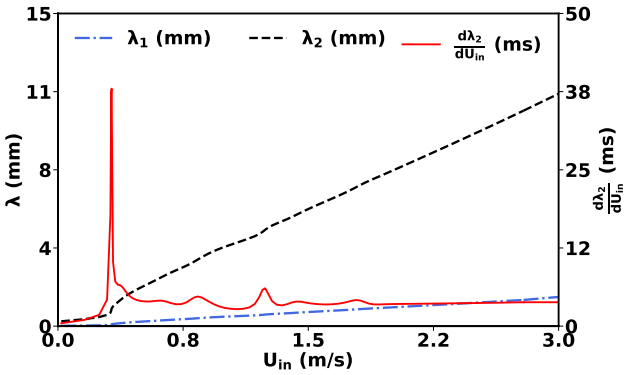

Fig. 2: (Blue) Position of the cool ignition front away from the inlet, λ_1, vs. inlet velocity, U_{in}. (Black) Position of the hot ignition front away from the inlet, λ_2, vs. inlet velocity, U_{in}. (Red) Derivative of the hot ignition front position with respect to the inlet velocity, $d\lambda_2/dU_{in}$ vs. U_{in}

4.2 Instantaneous flame structure

In the present study, the cool and the hot ignition fronts were identified by defining a progress variable, c as: $c = 1 - (T_b - T)/(T_b - T_u)$ where, T is the temperature at any point, T_u is the unburnt gas temperature and T_b is the burnt gas temperature. The value of c corresponding to the maximum heat release rate in the cool and the hot ignition front under laminar conditions was selected as the iso-contour representing the cool and the hot ignition front respectively. Here, the respective peaks were observed to occur at c = 0.05 and c = 0.85. Figure 3 presents contours of instantaneous temperature in the cases with the smallest (480N/480R) and the largest (960N/960R) l_e respectively. First, it is seen that both, the cool ignition front as well as the hot ignition front experience turbulence wrinkling. Second, the amount of wrinkling experienced by the cool ignition front in cases 480N/480R as well as 960N/960R is comparable. However, there is a considerable variation in the amount of wrinkling that the hot ignition front undergoes for a given value of l_e. Pre-ignition in the upstream mixture substantially increases the wrinkled length of the hot-ignition front. Single/multiple hot-spots are initially observed to occur ahead of the hot ignition front due to pre-ignition. Later, these hot-spots merge with the hot-ignition front giving rise to a single reaction front with a very large wrinkled length. At the same time, it is also noticed that the amount of wrinkling being experienced by the hot ignition front in the absence of pre-ignition is significantly lower.

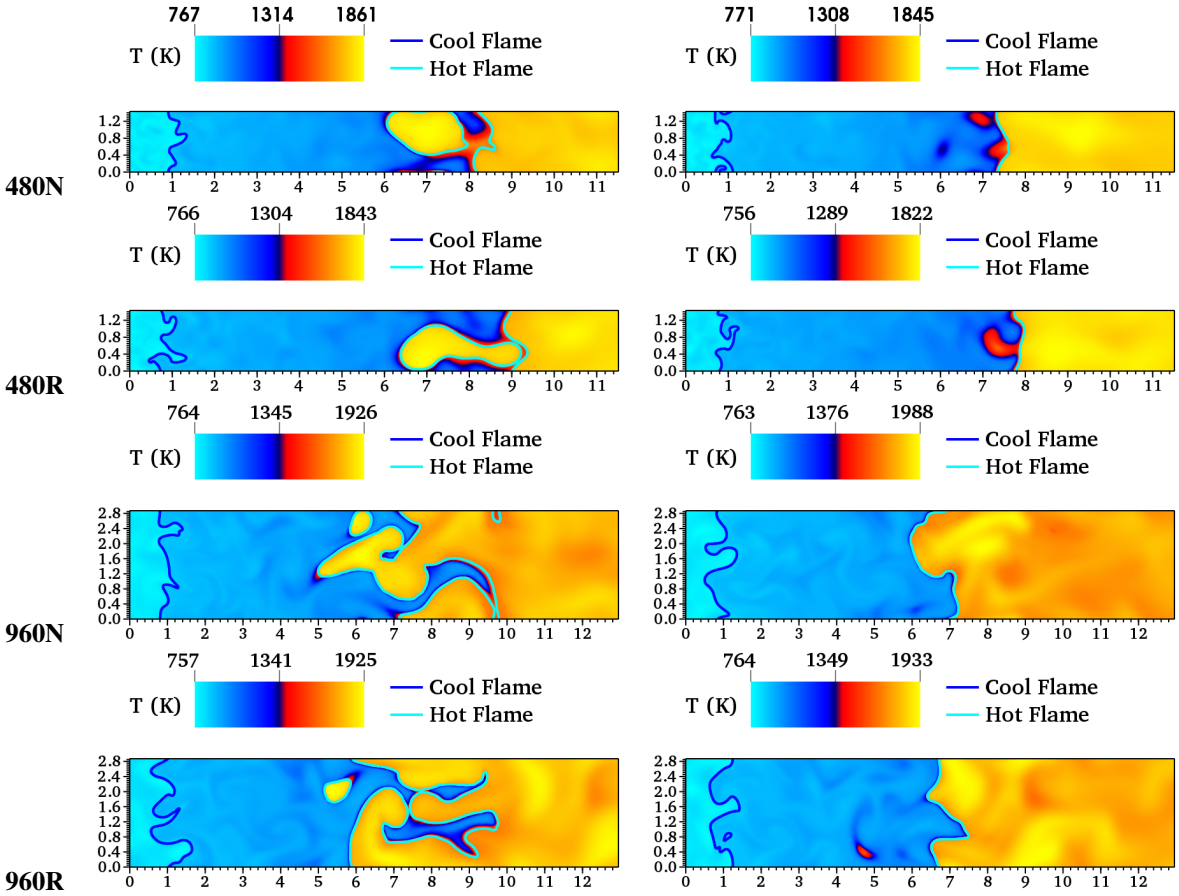

Fig. 3: Instantaneous temperature fields with iso-contours c = 0.05 (blue) and c = 0.85 (cyan) superimposed. Instantaneous temperature fields with maximum wrinkling of the hot ignition front are shown in the left sub-figures whereas the ones with minimum wrinkling of the hot ignition front are shown in the right sub-figures.

4.3 Mean flame structure

Figure 4 presents the mean heat release rate (HRR) as well as the reaction rates of key species conditioned on temperature. First, it is seen that with an increase in stratification/turbulence length scales, the profiles are lowered in magnitude, narrowed in temperature space and the corresponding peaks are shifted to lower temperatures. Second, the profiles in each case are found to be different from the initial laminar profiles. At the shortest stratification/turbulence length scale (cases 480N/480R), it is seen that the profiles closely match the laminar profile of a reaction front propagating at a much lower speed S = 0.71 m/s under identical unburnt mixture conditions. Based on S_T = 2 m/s, the turbulent cool as well as the hot reaction front was a priori expected to be controlled by ignition in each case. But, the profiles of CH_3OCH_2OH (product of LTC) and CO_2 (product of HTC) are seen to resemble more to a self-propagating flame. As the stratification/turbulence length scales are increased, unlike CH_3OCH_2OH, the profiles of CO_2 further shift towards that of a laminar flame propagating even slower at S = 0.38 m/s under identical unburnt mixture temperature but leaner conditions. Finally, at a given stratification/turbulence length scale, the effect of T-ϕ correlation on the flame structure is found to be marginal.

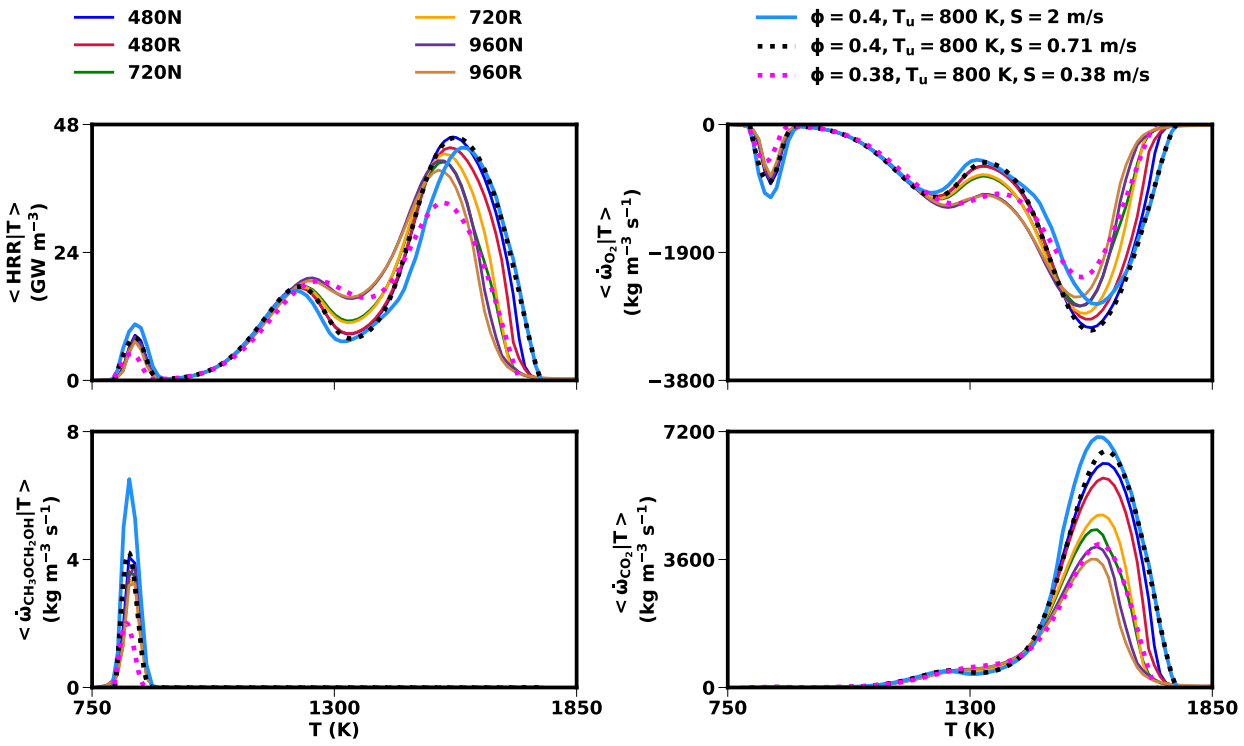

Fig. 4: Mean heat release rate, reaction rates of O_2, CH_3OCH_3, CH_3OCH_2OH and CO_2 conditional on the temperature compared to the laminar cases. T_u represents the unburnt mixture temperature.

4.4 Global burning velocity

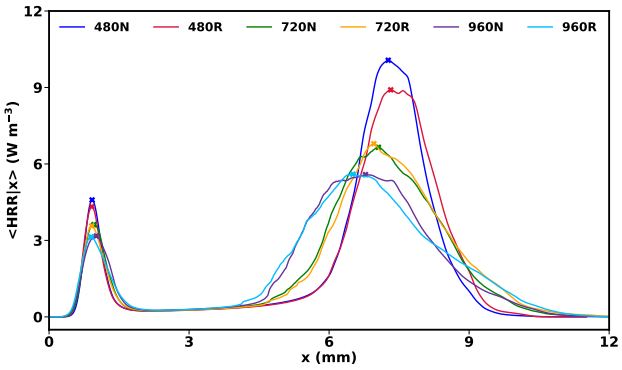

Fig. 5: Mean heat release rate conditional on the horizontal spatial location

The individual contributions from increase in length (A') and from the increase in burning rate per unit length of the flame (I_0) to the overall burning rate of the cool as well as the hot ignition front were determined as: $S_T/S_{1D} = I_0 \cdot A'$, where $A' = L_{wrinkled}/L_{flat}$. In each case, the mean turbulent flame speed, S_T = 2 m/s. As discussed earlier, the iso-surface c = 0.05 represents the mean turbulent cool reaction front while the iso-surface c = 0.85 represents the mean hot reaction front. Also, L_{flat} (= L_y) denotes the length of an unwrinkled cool/hot reaction front while $L_{wrinkled}$ denotes the length of a wrinkled cool/hot reaction front. Accordingly, two values of A', i.e. A'_{hot}

Case	λ_1 (mm)	λ_2 (m/s)	$S_{1D,cool}$	$S_{1D,hot}$	A'_{cool}	A'_{hot}	$I_{0,cool}$	$I_{0,hot}$
480N	0.92	7.27	2.04	1.95	1.79	2.71	0.55	0.38
480R	0.92	7.32	2.04	1.96	1.98	2.98	0.5	0.34
720N	0.96	7.06	2.14	1.89	1.80	3.86	0.52	0.27
720R	0.92	6.96	2.04	1.86	2.04	3.78	0.48	0.28
960N	1.01	6.78	2.26	1.81	1.71	4.42	0.52	0.25
960R	0.9	6.51	2.02	1.75	1.87	4.85	0.53	0.24

Table 2: Individual contributions of L' and I_0 to S_T in the respective cases.

and A'_{cool} were evaluated. Similarly, two values of S_{1D}, i.e. $S_{1D,hot}$ and $S_{1D,cool}$ were determined. This was achieved by first evaluating mean HRR conditional on the horizontal spatial location (x) and then determining the location of peak mean HRR as shown in Figure 5. Results obtained after time-averaging over multiple time-snap shots are listed in Table. 2. It is found that as the stratification/turbulence length scales are increased, λ_2 shifts towards the inlet which results in a decrease in the magnitude of $S_{1D,hot}$. On the other hand, λ_1 shifts marginally away from the inlet which causes a small rise in the magnitude of $S_{1D,cool}$. While A'_{hot} is noticed to progressively increase, A'_{cool} is found to remain fairly constant which is consistent with the earlier observations in Figure 3. Consequently, there is a marginal decrease in $I_{0,hot}$ whereas there is no significant change in $I_{0,cool}$. As before, the T-ϕ correlation in the respective cases doesn't seem to significantly affect either the amount of wrinkling or the increase in burning rate per unit length. The individual contributions of deflagration vis-á-vis spontaneous ignition to A' as well as I_0 is a subject of current investigation and will be presented elsewhere.

5. Conclusions

A 2D statistically stationary turbulent premixed flame propagating in a stratified DME/air mixture exhibiting two-staged ignition was simulated. Results obtained using different stratification/turbulent length scales and T-ϕ correlation showed that unlike the latter, the former parameter predominantly affects the turbulent flame dynamics. At shorter length-scales, the mean flame structure in temperature space was found to approach that of the self-propagating laminar flames under identical unburnt mixture conditions. At larger length scales, however, the mean flame structure was seen to approach that of the of the self-propagating laminar flames at identical unburnt temperature but leaner conditions. A global analysis of the flame burning velocity indicated that the mean turbulent hot reaction front shifts towards the inlet with an increase in the stratification/turbulence length scale. Meanwhile, the variation in the position of the mean turbulent cool reaction with respect to the imposed length scales was found to be marginal. Additionally, the hot ignition front was found to undergo considerably higher amount of wrinkling than the cool ignition front, predominantly due to pre-ignition in the upstream mixture. As a result, there was a marginal decrease in the burning efficiency factor of the hot reaction front whereas there was no noticeable change in the burning efficiency factor of the cool reaction front.

6. Acknowledgements

This work was supported by King Abdullah University of Science and Technology (KAUST). This research used resources of the Oak Ridge Leadership Computing Facility (OLCF) and the Compute and Data Environment for Science (CADES) at ORNL, which is supported by the Office of Science of the U.S. Department of Energy under Contract No. DE-AC05-00OR22725.

References

[1] C. Strozzi, A. Mura, J. Sotton, and M. Bellenoue, Experimental analysis of propagation regimes during the autoignition of a fully premixed methane−air mixture in the presence of temperature inhomogeneities, Combustion and Flame 159 (2012) 3323–3341.

[2] D. Assanis, S. W. Wagnon, and M. S. Wooldridge, An experimental study of flame and autoignition interactions of iso-octane and air mixtures, Combustion and Flame 162 (2015) 1214–1224.

[3] S. Lapointe and G. Blanquart, Fuel and chemistry effects in high Karlovitz premixed turbulent flames, Combustion and Flame 167 (2016) 294–307.

[4] N. Fogla, F. Creta, and M. Matalon, The turbulent flame speed for low-to-moderate turbulence intensities: Hydrodynamic theory vs. experiments, Combustion and Flame 175 (2017) 155–169.

[5] T. Nilsson, H. Carlsson, R. Yu, and X.-S. Bai, Structures of turbulent premixed flames in the high Karlovitz number regime–DNS analysis, Fuel 216 (2018) 627–638.

[6] J. Rosell, X.-S. Bai, J. Sjoholm, B. Zhou, Z. Li, Z. Wang, P. Pettersson, Z. Li, M. Richter, and M. Alden, Multi-species PLIF study of the structures of turbulent premixed methane/air jet flames in the flamelet and thin-reaction zones regimes, Combustion and Flame 182 (2017) 324–338.

[7] T. M. Wabel, A. W. Skiba, J. E. Temme, and J. F. Driscoll, Measurements to determine the regimes of premixed flames in extreme turbulence, Proceedings of the Combustion Institute 36 (2017) 1809–1816.

[8] H. Kobayashi, T. Nakashima, T. Tamura, K. Maruta, and T. Niioka, Turbulence measurements and observations of turbulent premixed flames at elevated pressures up to 3.0 MPa, Combustion and flame 108 (1997) 104–117.

[9] C. Rutland and A. Trouvé, Direct simulations of premixed turbulent flames with nonunity Lewis numbers, Combustion and Flame 94 (1993) 41–57.

[10] M. J. Dunn and R. S. Barlow, Effects of preferential transport and strain in bluff body stabilized lean and rich premixed CH4/air flames, Proceedings of the Combustion Institute 34 (2013) 1411–1419.

[11] G. J. Smallwood, Ö. Gülder, D. R. Snelling, B. Deschamps, and I. Gökalp, Characterization of flame front surfaces in turbulent premixed methane/air combustion, Combustion and Flame 101 (1995) 461–470.

[12] Z. Wang, E. Motheau, and J. Abraham, Effects of equivalence ratio variations on turbulent flame speed in lean methane/air mixtures under lean-burn natural gas engine operating conditions, Proceedings of the Combustion Institute 36 (2017) 3423–3430.

[13] S. Lapointe, B. Savard, and G. Blanquart, Differential diffusion effects, distributed burning, and local extinctions in high Karlovitz premixed flames, Combustion and flame 162 (2015) 3341–3355.

[14] B. Savard, S. Lapointe, and A. Teodorczyk, Numerical investigation of the effect of pressure on heat release rate in iso-octane premixed turbulent flames under conditions relevant to SI engines, Proceedings of the Combustion Institute 36 (2017) 3543–3549.

[15] N. Peters, Turbulent combustion, Cambridge university press, 2000.

[16] M. P. Musculus, P. C. Miles, and L. M. Pickett, Conceptual models for partially premixed low-temperature diesel combustion, Progress in energy and combustion science 39 (2013) 246–283.

[17] Y. Ju, W. Sun, M. P. Burke, X. Gou, and Z. Chen, Multi-timescale modeling of ignition and flame regimes of n-heptane-air mixtures near spark assisted homogeneous charge compression ignition conditions, Proceedings of the Combustion Institute 33 (2011) 1245–1251.

[18] S. Desai, R. Sankaran, and H. G. Im, Unsteady deflagration speed of an auto-ignitive dimethyl-ether (DME)/air mixture at stratified conditions, Proceedings of the Combustion Institute 37 (2019) 4717–4727.

[19] S. H. Won, B. Windom, B. Jiang, and Y. Ju, The role of low temperature fuel chemistry on turbulent flame propagation, Combustion and Flame 161 (2014) 475–483.

[20] B. Windom, S. H. Won, C. B. Reuter, B. Jiang, Y. Ju, S. Hammack, T. Ombrello, and C. Carter, Study of ignition chemistry on turbulent premixed flames of n-heptane/air by using a reactor assisted turbulent slot burner, Combustion and Flame 169 (2016) 19–29.

[21] B. Savard, H. Wang, A. Teodorczyk, and E. R. Hawkes, Low-temperature chemistry in n-heptane/air premixed turbulent flames, Combustion and Flame 196 (2018) 71–84.

[22] S. Deng, P. Zhao, M. E. Mueller, and C. K. Law, Stabilization of laminar nonpremixed DME/air coflow flames at elevated temperatures and pressures, Combustion and Flame 162 (2015) 4471–4478.

[23] A. Krisman, E. R. Hawkes, M. Talei, A. Bhagatwala, and J. H. Chen, Polybrachial structures in dimethyl ether edge-flames at negative temperature coefficient conditions, Proceedings of the Combustion Institute 35 (2015) 999–1006.

[24] D. G. Goodwin, H. K. Moffat, and R. L. Speth, Cantera: An Object-oriented Software Toolkit for Chemical Kinetics, Thermodynamics, and Transport Processes, 2016, URL: `www.cantera.org`.

[25] C. S. Yoo and H. G. Im, Characteristic boundary conditions for simulations of compressible reacting flows with multi-dimensional, viscous and reaction effects, Combustion Theory and Modelling 11 (2007) 259–286.

[26] A. Krisman, E. R. Hawkes, and J. H. Chen, The structure and propagation of laminar flames under autoignitive conditions, Combustion and Flame 188 (2018) 399–411.

[27] T. Passot and A. Pouquet, Numerical simulation of compressible homogeneous flows in the turbulent regime, Journal of Fluid Mechanics 181 (1987) 441–466.

[28] M. B. Luong, R. Sankaran, G. H. Yu, S. H. Chung, and C. S. Yoo, On the effect of injection timing on the ignition of lean PRF/air/EGR mixtures under direct dual fuel stratification conditions, Combustion and Flame 183 (2017) 309–321.

[29] J. H. Chen, E. R. Hawkes, R. Sankaran, S. D. Mason, and H. G. Im, Direct numerical simulation of ignition front propagation in a constant volume with temperature inhomogeneities: I. Fundamental analysis and diagnostics, Combustion and flame 145 (2006) 128–144.

[30] Y. Wang and C. Rutland, Effects of temperature and equivalence ratio on the ignition of n-heptane fuel spray in turbulent flow, Proceedings of the Combustion Institute 30 (2005) 893–900.

[31] F. E. Hernández Pérez, N. Mukhadiyev, X. Xu, A. Sow, B. J. Lee, R. Sankaran, and H. G. Im, Direct numerical simulations of reacting flows with detailed chemistry using many-core/GPU acceleration, Computers & Fluids 173 (2018) 73–79.

[32] S. Desai, Y. J. Kim, W. Song, M. Luong, F. H. Pérez, R. Sankaran, and H. G. Im, Direct numerical simulations of reacting flows with contact discontinuities and stiff chemistry using many-core/GPU acceleration, (2018), Submitted to special issue of the 30th International Conference on Parallel Computational Fluid Dynamics.

[33] K. N. C. Bray, Studies of the turbulent burning velocity, Proc. R. Soc. Lond. A 431 (1990) 315–335.

[34] S. M. Candel and T. J. Poinsot, Flame stretch and the balance equation for the flame area, Combustion Science and Technology 70 (1990) 1–15.